

# High Temperature Oxidation Behavior of Nickel and Iron Based Superalloys in Helium Containing Trace Impurities

C. J. Tsai<sup>1</sup>, T. K. Yeh<sup>1</sup>, and M. Y. Wang<sup>2,†</sup>

<sup>1</sup>Dept. of Engineering and System Science, National Tsing Hua University, 101, Sec. 2, Kuangfu Rd., Hsinchu 300 Taiwan

<sup>2</sup>Nuclear Science and Technology Development Center, National Tsing Hua University, 101, Sec. 2, Kuangfu Rd., Hsinchu 300 Taiwan

(Received December 18, 2018; Revised January 23, 2019; Accepted January 24, 2019)

A high-temperature gas-cooled reactor (HTGR) is recognized as the best candidate reactor for next generation nuclear reactors. Helium is used to be the coolant in the core of the HTGR with temperature expected to exceed 900 °C at the core outlet. Several iron- and nickel-based superalloys, including Alloy 800H, Hastelloy X, and Alloy 617, are potential structural materials for intermediate heat exchanger (IHX) in an HTGR. Oxidation behaviors of three selected alloys (Hastelloy X, Alloy 800H, and Alloy 617) were investigated at four different temperatures from 650°C to 950 °C under helium environments with various concentrations of O<sub>2</sub> and H<sub>2</sub>O. Preliminary results showed that chromium oxide as the primary protective layer was observed on surfaces of the three tested alloys. Based on results of mass gain and SEM analyses, Hastelloy X alloy exhibited the best corrosion resistance in all corrosion tests. Further details on the oxidation mechanism of these alloys are presented in this study.

**Keywords:** HTGR, Superalloys, Oxidation, Corrosion, Helium gas

## 1. Introduction

A high-temperature gas-cooled reactor (HTGR) is a Generation IV nuclear reactor based on the design developed in the 1950s. This type of system is designed to attain the aim of high efficiency and produce massive amounts of hydrogen. An inert gas, helium, is used in the coolant system and the outlet temperature exceeds 900 °C [1]. Accordingly, the alloy materials selected for an intermediate heat exchanger (IHX) in an HTGR should have high degradation resistance and superior mechanical strength over a long lifetime, about 60 years. The helium used in HTGR coolant system predictably contains low levels of impurities during reactor operation. Impurities in the helium coolant, such as oxygen and water vapor, may increase the corrosion rate of alloys at high temperatures [2-7]. Several nickel- and iron-based alloys are potential candidates for structural materials in an HTGR. Furthermore, more severe oxidation of the alloys used for IHX could result in integrity breach of the IHX structure during an air ingress event. Although the formation of stable oxides is preferred for preventing more oxygen from reacting with substrate to degrade alloy materials,

unexpected spallation of thick oxides may harm the long-term integrity and hence the mechanical strength of the materials during prolonged operation of an HTGR. In this study, two nickel-based alloys (Hastelloy X and Alloy 617) and one iron-based alloy (Alloy 800H) were selected as target materials for undergoing corrosion test in helium gas environments with various amounts of impurities (i.e. oxygen and water vapor) at different temperatures from 650 °C to 950 °C for 48h. Tests results on the mass changes, surface morphologies, and composition of oxides of the samples are reported.

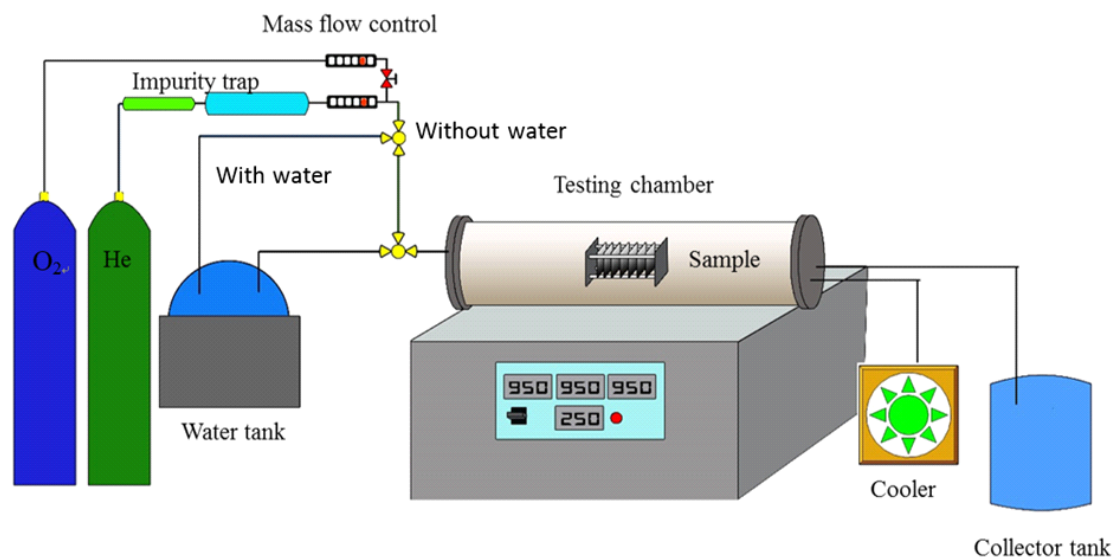
## 2. Materials

Table 1 shows the chemical composition of the tested materials of Alloy 800H, Hastelloy X, and Alloy 617. These alloys were cut into samples in square disk shape with a dimension of 20 mm × 20 mm × 1 mm. No thermal treatment was carried out before the corrosion test. Both sides of the samples were mechanically polished by abrasive paper starting from 80 grit up to 1200 grit. Before undergoing corrosion test, the specimens were ultrasonically washed in acetone (CH<sub>3</sub>COCH<sub>3</sub>), dried in air, and weighted using an electronic balance.

<sup>†</sup> Corresponding author: meywang@mx.nthu.edu.tw

**Table 1 Chemical composition of the alloys used in this study (wt%)**

Alloy	Ni	Fe	Cr	Al	Mo	Mn	Ti	C	Co	W	Cu	Si
Alloy 800H	31.7	bal	21.4	.4	-	1.5	.4	.05	-	-	.75	1.0
Hastelloy X	Bal	22	18	-	9	1	-	.1	1.5	.6	-	1
Alloy 617	Bal	.9	21.6	1.2	9.5	.1	.3	.06	12.5	-	.5	.01

**Fig. 1 Conceptual Schematic of the experimental system.****Table 2 Level of impurities (ppm) of pure helium gas used in this study (He > 99.9995%)**

Impurity	CO	CO <sub>2</sub>	H <sub>2</sub>	H <sub>2</sub> O	N <sub>2</sub>	O <sub>2</sub>	CH <sub>4</sub>
Level(ppm)	< 0.05	< 0.05	< 0.05	0.58	0.80	0.20	< 0.05

### 3. Experiment

#### 3.1 Test loops

A conceptual schematic of the experimental system is shown in Fig. 1. In each corrosion test, six samples, two from each alloy, were exposed to designated flowing gas mixtures in a high-temperature quartz tube furnace. The sample holder was made of ceramic, which is an inert material. Gas input was controlled using a mass flow controller set with a flow rate of 250 ml/min. The samples were heated up at a rate of 15 °C/min and cooled down at a rate of 7.5 °C/min in pure argon at a constant flow rate of 250 ml/min.

#### 3.2 Test conditions

The experiments in this study used six gaseous conditions to simulate normal and various air-ingress environments in an HTGR, including pure dry helium, 99% heli-

um with 1% oxygen, 90% helium with 10% oxygen, 90% helium with 10% air, pure helium with 10% humidity, and pure helium with 50% humidity. Table 2 lists the impurity levels in pure helium used in this study. The testing temperature was set at 650 °C, 750 °C, 850 °C, and 950 °C in each experimental condition. Corrosion test duration was 48 hours.

#### 3.3 Sample Observation and Analyses

After the corrosion tests, the mass gain of each sample was measured using a high-precision balance. A scanning electron microscope (SEM) was used to analyze the oxides on the surface and cross-sectional microstructure of samples in different conditions. The elemental composition of the oxide was analyzed using energy-dispersive X-ray spectroscopy (EDX). The crystal structure and chemical composition of oxide were characterized by X-ray diffraction (XRD), confirming the results of EDX.

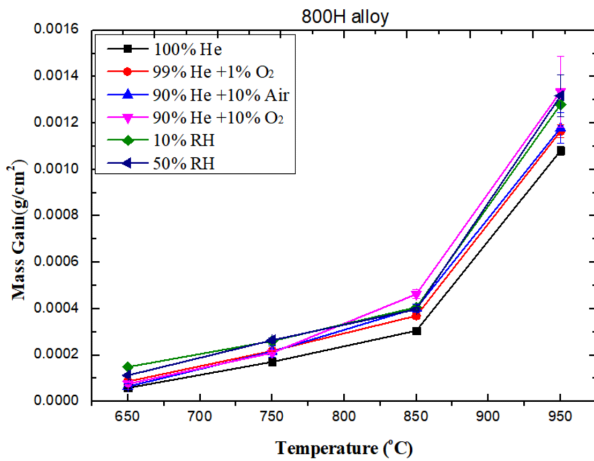


Fig. 2 Mass gains of Alloy 800H at various testing conditions.

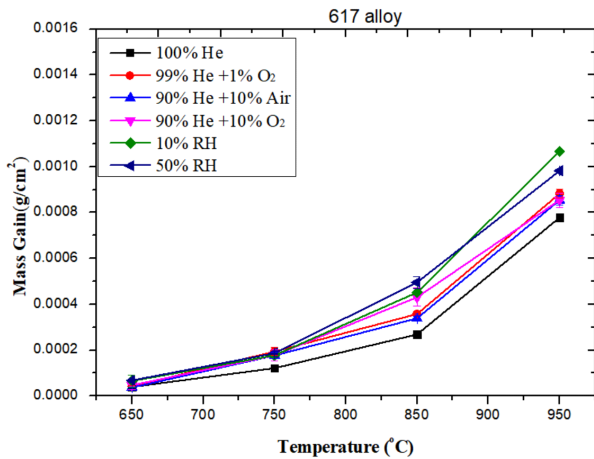


Fig. 3 Mass gains of Alloy 617 at various testing conditions.

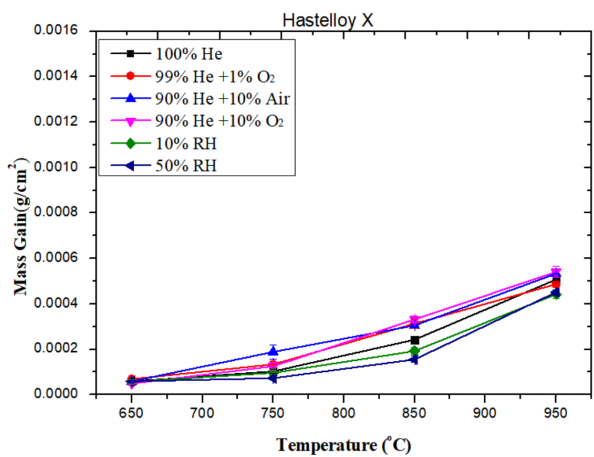


Fig. 4 Mass gains of Hastelloy X at various testing conditions.

## 4. Result and Discussion

### 4.1 Mass gain in high-temperature gas environments

Fig. 2 shows the mass gains of Alloy 800H as a function

of the test temperature after isothermal oxidation up to 48 hours in various controlled helium environments. Similar oxidation behavior appeared at 650 °C, 750 °C and 850 °C in all gas environments, and no significant differences in mass gain of this alloy were observed. The oxidation rate at 950 °C exhibited higher than those at other temperatures. At 850 °C, the mass gain of Alloy 800H in 90% helium with 10% oxygen was the highest due to the higher oxygen partial pressure. As up to 950 °C, the mass gains in both wet 10% and 50% humidity environments were similar with that in 90% helium with 10% oxygen. No oxide spallation was observed on the surface of Alloy 800H in this study.

Fig. 3 shows the mass gain of Alloy 617 after being oxidized at four test temperatures up to 48 hours in various controlled helium environments. It is known that the alloy oxidation is faster in water vapors or humid environments than in dry environments, therefore, a higher mass gain is expected in wet helium than in the helium environment containing air or oxygen at the same temperature.

Fig. 4 indicated that Hastelloy X had the same tendency of oxidation behavior at various temperatures from 650 °C to 950 °C. At four test temperatures, a lower mass gain in both humid environments. The lack of obvious spallation on the surface suggested that the major source of lower mass gain might be caused by the evaporation of Cr-rich oxide layers, which become unstable and react with water vapors [8-14]. Hastelloy X apparently has the ability to resist oxidation at high temperatures, but chromic volatilization may occur in humid environments. Furthermore, the mass gain of Alloy 800H was the highest, and that of Hastelloy X was the lowest among the three alloys under all test conditions.

### 4.2 Morphology of Alloy 800H

Fig. 5 shows the cross-sectional oxide morphologies of Alloy 800H tested at 950 °C for 48 hours in pure dry helium, 99% helium with 1% oxygen, 90% helium with 10% oxygen, 90% helium with 10% air, pure helium with 10% humidity, and pure helium with 50% humidity. Fig. 6 shows the EDX mapping analysis of Alloy 800H for 48 hours at 950 °C in a 90% helium with 10% oxygen environment. The elements of iron, chromium, and manganese appear in the oxide layer of Alloy 800H, and Cr-rich oxide forms an inner layer above the substrate. The scattered internal oxides of Al<sub>2</sub>O<sub>3</sub> were observed beneath the continuous Cr<sub>2</sub>O<sub>3</sub> layer. Because manganese is soluble in Cr<sub>2</sub>O<sub>3</sub> at high temperature, it exists in the inner oxide layer to forms manganese spinel, which is more stable than MnO and Cr<sub>2</sub>O<sub>3</sub>, at the interface of chromium oxide and the spinel phase [15,16]. Furthermore, man-

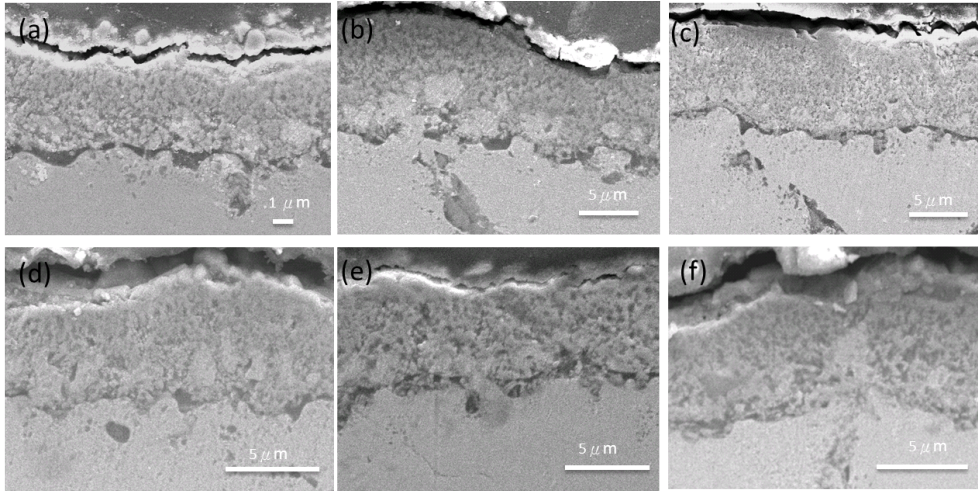


Fig. 5 SEM cross-sectional micrographs for Alloy 800H at 950 °C for 48 hours: (a) in 100% pure dry helium, (b) in 99% helium with 1% oxygen, (c) in 199% helium with 10% air, (d) in 99% helium with 10% oxygen, (e) in pure helium with 10% humidity, (f) in pure helium with 50% humidity.

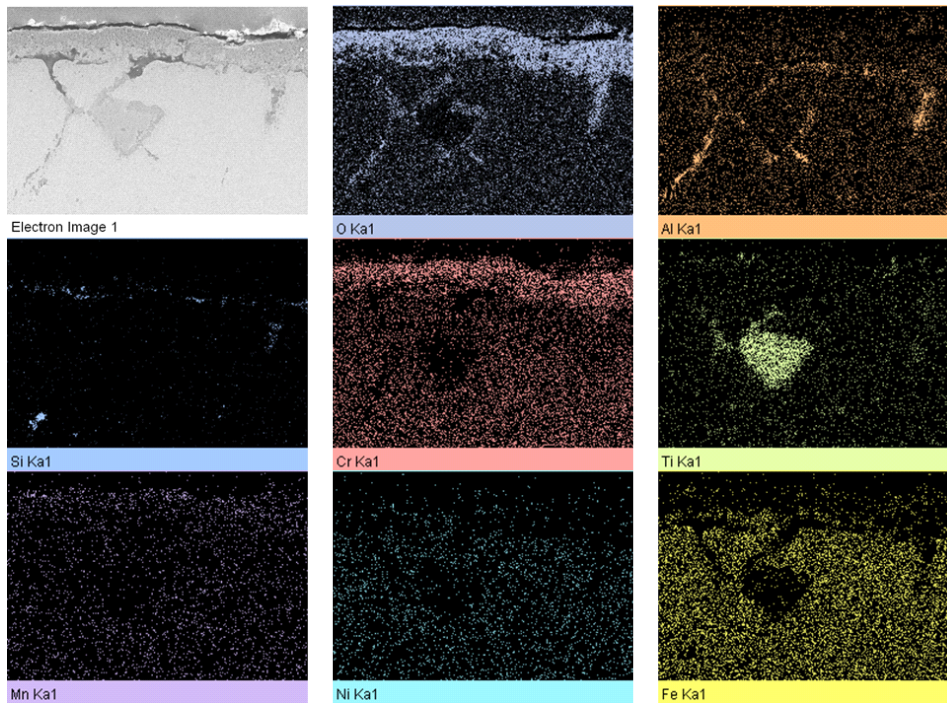


Fig. 6 EDX mapping for the cross-sectional of Alloy 800H at 950 °C for 48 hours in a 90% helium with 10% oxygen environment.

ganese diffuses faster than iron or nickel in the  $\text{Cr}_2\text{O}_3$  layer via the lattice diffusion, which explains how manganese concentrates on top of the spinel scale [17,18]. Thus, three oxide layers were formed by a spinel phase ( $\text{NiFeO}_4$ ,  $\text{MnCr}_2\text{O}_4$ ,  $\text{Mn}_3\text{O}_4$  and  $\text{Fe}_3\text{O}_4$ ) on the surface, a  $\text{Cr}_2\text{O}_3$  layer below the external oxide layer, and an internal oxide of an  $\text{Al}_2\text{O}_3$  layer below the chromium-rich layer. These oxides were confirmed by XRD and EDX analysis.

EDX analysis also confirmed the depletion of chromium in the matrix as  $\text{Cr}_2\text{O}_3$  grew on the top of the metal.

#### 4.3 Morphology of Alloy 617

Fig. 7 shows SEM cross-sectional micrographs of Alloy 617 at 950 °C for 48 hours in various controlled helium environments. The EDX mapping analysis of Alloy 617 for 48 hours at 950 °C in a 90% helium with 10% oxygen environment is shown in Fig. 8. Titanium and manganese

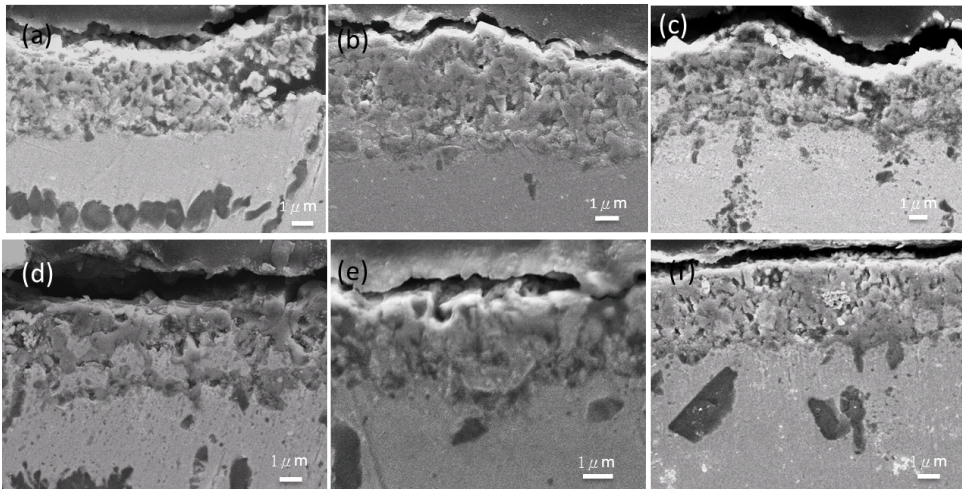


Fig. 7 SEM cross-sectional micrographs for Alloy 617 at 950 °C for 48 hours: (a) in 100% pure dry helium, (b) in 99% helium with 1% oxygen, (c) in 199% helium with 10% air, (d) in 99% helium with 10% oxygen, (e) in pure helium with 10% humidity, (f) in pure helium with 50% humidity.

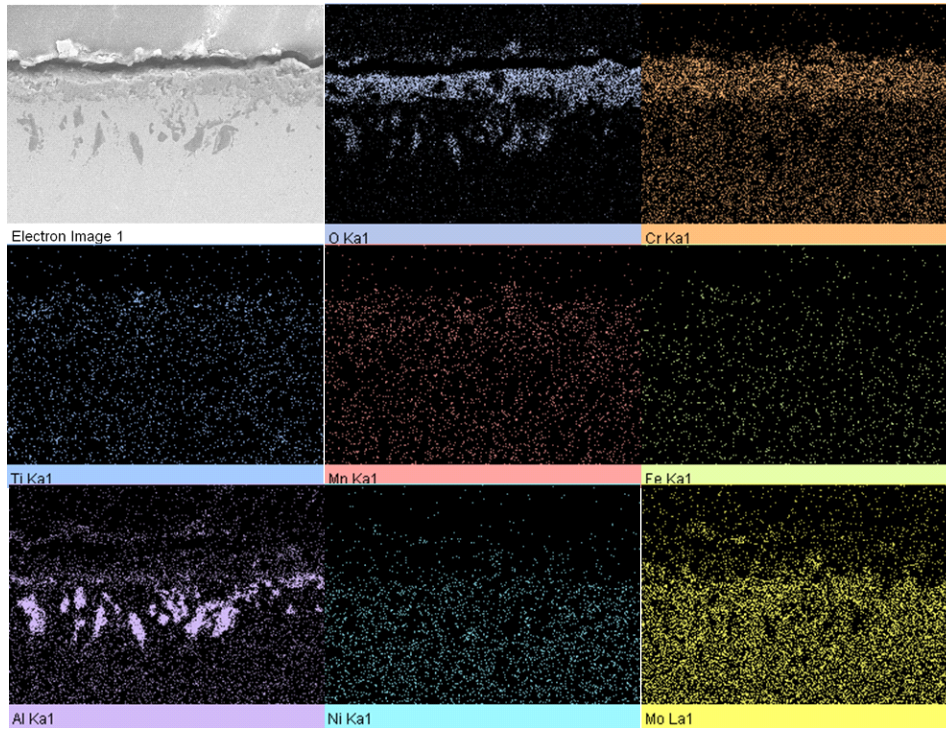


Fig. 8 EDX mapping the cross-sectional of Alloy 617 at 950 °C for 48 hours in a 90% helium with 10% oxygen environment.

existed on the top layer of the oxide in the form of  $\text{TiO}_2$  and  $\text{MnCr}_2\text{O}_4$ , as confirmed by XRD analysis. The surface oxides of Alloy 800H and Hastelloy X exhibited the chromium oxide formed as  $\text{Cr}_2\text{O}_3$ . It was noted that aluminum particles concentrated below the metal-scale interface as Al-oxide or  $\text{Al}_2\text{O}_3$ . Therefore, during the SEM, XRD, and EDX analysis, three oxide layers were formed by a layer of spinel phase and  $\text{TiO}_2$  on the top surface, an inner oxide

layer consisting of  $\text{Cr}_2\text{O}_3$  below the spinel, and aluminum concentrating in the metal layer, forming  $\text{Al}_2\text{O}_3$  internal oxidation.

#### 4.4 Morphology of Hastelloy X

Fig. 9 shows SEM cross-sectional micrographs of Hastelloy X tests at 950 °C for 48 hours in various controlled helium environments. The SEM micrographs of

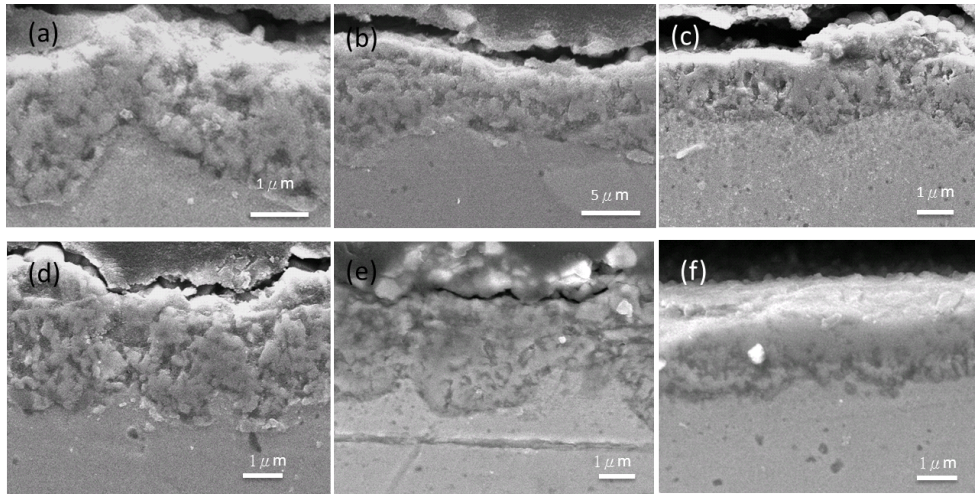


Fig. 9 SEM cross-sectional micrographs for Hastelloy X at 950 °C for 48 hours: (a) in 100% pure dry helium, (b) in 99% helium with 1% oxygen, (c) in 199% helium with 10% air, (d) in 99% helium with 10% oxygen, (e) in pure helium with 10% humidity, (f) in pure helium with 50% humidity.

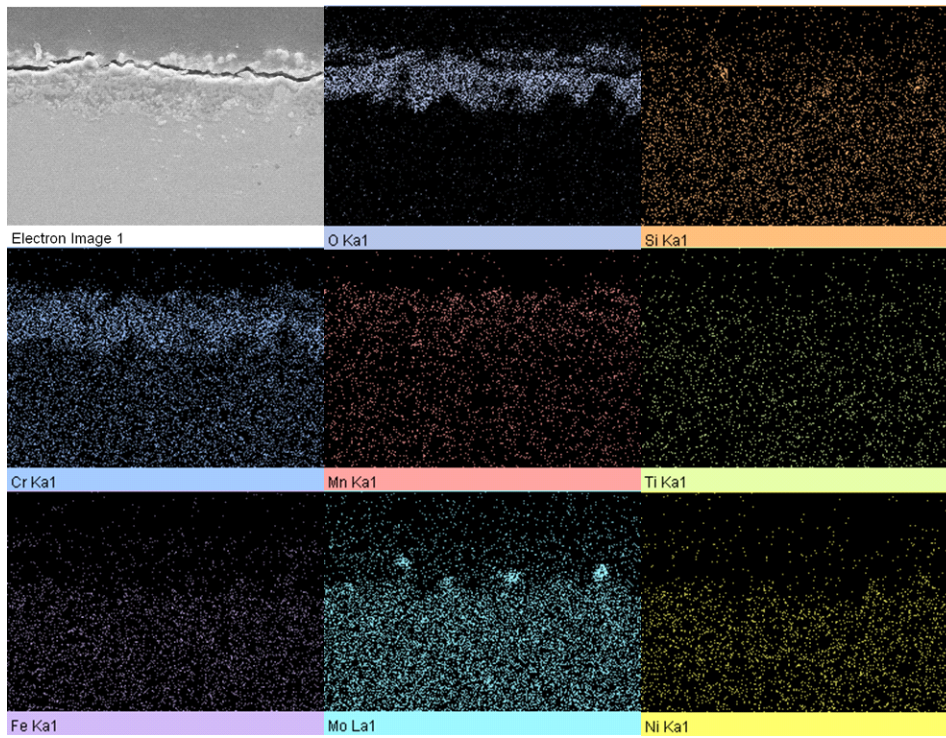


Fig. 10 EDX mapping for the cross-sectional of Hastelloy X at 950 °C for 48 hours in a 90% helium with 10% oxygen environment.

this alloy in various gas conditions appear similar, and it is consistent with the results of mass gain. According to the EDX mapping analysis of the sample shown in Fig. 10, which shows the results tested at 950 °C for 48 hours in a 90% helium with 10% oxygen environment, the oxide on the surface consists of an inner layer of  $\text{Cr}_2\text{O}_3$ , and silicon collects below the  $\text{Cr}_2\text{O}_3$  inner layer. The manganese exists in both the inner and outer oxide

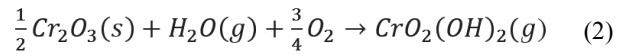
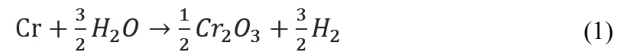
layers since Mn diffuses faster than Cr, Fe, and Ni and is solute in  $\text{Cr}_2\text{O}$  layer [17,18]. Furthermore, manganese oxide forms a stable spinel phase, and co-exist with  $\text{Cr}_2\text{O}_3$  [15,16]. Conversely, Fe and Ni are mostly blocked in the matrix by  $\text{Cr}_2\text{O}_3$  even though in severe condition. Due to the results of XRD and EDX analysis, the oxide layer was mainly composed of a thin spinel layer composed of  $\text{MnCr}_2\text{O}_4$  on the surface, a  $\text{Cr}_2\text{O}_3$  layer that accounts

for most of the oxides above the substrate, and silicon forming an internal oxide as SiO<sub>2</sub> below the chromium-rich layer.

#### 4.5 Corrosion mechanism

The composition of elements is very crucial to deciding the properties and characteristics of an alloy. Alloys may maintain long-term integrity exposed to high temperature gas environments due to the presence of a protective oxide layer on the alloy surface. This avoids or reduces the diffusion rate of anions inward to the metal or cation outward to the surface [19]. In this study, Alloy 800H is iron-based alloy, and Hastelloy X and Alloy 617 are nickel-based alloys. The Cr contents in the selected alloys ranged from 18% to 22%, which surpass the minimum value of critical chromium concentration to form continuous oxide scales [8,20-22]. Because chromium oxide grows at a slow rate and is considerably more stable than oxides of iron, nickel, and cobalt, Cr<sub>2</sub>O<sub>3</sub> is formed preferentially based on thermodynamics [19]. Therefore, a Cr<sub>2</sub>O<sub>3</sub> layer became the major structure on the surface of the tested alloy at the early stage of the corrosion process. The concentration of aluminum in the tested alloys in this study was less than 2% and prevent it from forming scales even if Al<sub>2</sub>O<sub>3</sub> has a lower Gibbs free energy ( $\Delta G_f = -858.30$  kJ/mol) than that of Cr<sub>2</sub>O<sub>3</sub> ( $\Delta G_f = -546.86$  kJ/mol). In this case, the aluminum caused internal oxidation underneath the surface oxide layer, leading to reduction in creep resistance of the alloy due to the tensile stress in the perpendicular direction. Cr<sub>2</sub>O<sub>3</sub> would be the main protective oxide, and the internal oxidation of Al would cause alloy failure [19].

Alloy oxidation becomes faster in the wet helium environments compared to pure air helium and the helium environment containing oxygen or air. This study shows that the mass gain of Alloy 617 in wet helium environments was greater than in a mixture of helium and oxygen at 850 °C and 950 °C, and the variation of mass gain in all tested environments is not significant at 650 °C and 750 °C. Alloy 800H had a slightly higher mass gain in wet helium environments than the helium environment containing oxidants except 10% oxygen. For Hastelloy X, the mass gain in wet helium environments was smaller than that in pure dry helium and helium environment containing oxidants. Alloy in a humid helium environment may react with steam in several oxidizing ways. Steam may react with metal to produce oxide and hydrogen on the metal surface. Alternatively, this reaction produces volatile hydrated species [23,24]. For example, chromium may form Cr<sub>2</sub>O<sub>3</sub> and H<sub>2</sub> or CrO<sub>2</sub>(OH)<sub>2</sub>, as determined by the following reactions:



CrO<sub>2</sub>(OH)<sub>2</sub> is a volatile chromium oxide, and then reduce the mass gain of the alloy. Although FeO, Fe<sub>3</sub>O<sub>4</sub>, Fe<sub>2</sub>O<sub>3</sub>, NiO, and Al<sub>2</sub>O<sub>3</sub> also form volatile compounds by reacting with steam, the hydroxide formation reaction of Cr<sub>2</sub>O<sub>3</sub> has lower free energy than the above reactions, and CrO<sub>2</sub>(OH)<sub>2</sub> is more stable than other hydroxides [25,26]. At Fig. 9, the oxide thickness in the wet helium environments was thinner than those in other helium conditions. It was also found that a higher humid helium environment would reduce the mass gain of Hastelloy X. This can be explained by the formation of volatile chromium hydroxide on these alloys. The behavior of volatilization reduces the lifetime of alloys due to the thinner protective layer [19].

#### 5. Conclusion

In this study, isothermal oxidation tests on Alloy 800H, Hastelloy X, and Alloy 617 were conducted at different temperatures from 650 °C to 950 °C for 48 hours in six controlled helium environments. The alloys in this study are potential superalloys for an HTGR involving intermediate heat exchanger and recuperator applications. Based on the results of oxidation tests, SEM and XRD analyses, this study presents the following findings:

1. At 950 °C, a continuous Cr<sub>2</sub>O<sub>3</sub> layer was observed on the surfaces of all tested alloys in the six selected environments.
2. Hastelloy X exhibited the lowest mass gain in all test conditions among the tested alloys. This alloy exhibited the simultaneous formation of Cr<sub>2</sub>O<sub>3</sub> and MnCr<sub>2</sub>O<sub>4</sub> on the surface of the alloy. In the meantime, Hastelloy X demonstrated lower mass gains in humid helium environments than those in dry helium environments containing oxygen or dry air.
3. Both Alloy 800H and Alloy 617 suffered from internal oxidation after the oxidized test at 950 °C for 48 hours. Alloy 617 exhibited more aluminum oxides below the Cr<sub>2</sub>O<sub>3</sub> inner layer and a poorer resistance to internal oxidation.

## Acknowledgments

The authors (C. J. Tsai, T. K. Yeh, M. Y. Wang) greatly appreciate the use of facility at CNMM of the National Tsing Hua University which is partly supported by Atomic Energy Council, Republic of China (Taiwan) under the project accounting number AEC10411057L.

## References

1. NUREG/CR-6824, Materials Behavior in HTGR Environments (2003).
2. C. Jang, D. Lee, and D. Kim, *Int. J. Pres. Ves. Pip.*, **85**, 368 (2008).
3. C. Cabet and F. Rouillard, *J. Nucl. Mater.*, **392**, 235 (2009).
4. K. Mo, G. Lovicu, H. M. Tung, X. Chen, and J. F. Stubbins, *Proc. 18th International Conference on Nuclear Engineering*, p.052908-1, Xi'an Jiaotong University, Xi'an, China (2010).
5. N. Sakaba, S. Hamamoto, and Y. Takeda, *J. Nucl. Sci. Technol.*, **47**, 269 (2012).
6. J. Chapovaloff, D. Kaczorowski, and G. Girardin, *Mater. Corros.*, **59**, 584 (2008).
7. D. Kim, I. Sah, D. Kim, W. S. Ryu, and C. Jang, *Oxid. Met.*, **75**, 103 (2011).
8. P. Kofstad, *High Temperature Corrosion, 1st ed.*, ch. 12, Elsevier Applied Science, London (1988).
9. D. Caplan and M. Cohen, *Corrosion*, **15**, 57 (1959).
10. D. R. Sigler, *Oxid. Met.*, **46**, 335 (1996).
11. H. Nickel, Y. Wouters, M. Thiele and W. J. Quadackers, *Fresen. J. Anal. Chem.*, **361**, 540 (1998).
12. H. Asteman, J. E. Svensson, M. Norell and L. G. Johansson, *Oxid. Met.*, **54**, 11 (2000).
13. R. Pieraldi and B. A. Pint, *Oxid. Met.*, **61**, 463 (2004).
14. B. A. Pint and J. M. Rakowski, *Proc. CORROSION 2000*, Paper 00259, NACE International, Orlando, Florida, USA (2000).
15. A. D. Dalvi and D. E. Coates, *Oxid. Met.*, **5**, 113 (1972).
16. I. H. Jung, *Solid State Ionics*, **177**, 765 (2006).
17. A. Naoumidis, H. A. Schulze, W. Jungen and P. Lersch, *J. Eur. Ceram. Soc.*, **7**, 55 (1991).
18. P. A. Tempest and R. K. Wild, *Oxid. Met.*, **17**, 345 (1982).
19. D. J. Young, *High Temperature Oxidation and Corrosion of Metals, 1st ed.*, pp. 185-187 Elsevier, London (2008).
20. G. C. Wood, I. G. Wright, T. Hodgkiess and D. P. Whittle, *Werkst. Korros.*, **21**, 700 (1970).
21. G. S. Giggins and F. S. Pettit, *T. Metall. Soc. AIME*, **245**, 2495 (1969).
22. J. Croll and G. R. Wallwork, *Oxid. Met.*, **4**, 121 (1972).
23. N. Jacobson, D. Myers, E. Opila, and E. Copland, *J. Phys. Chem. Solids*, **66**, 471 (2005).
24. B. B. Ebbinghaus, *Combust. Flame*, **93**, 119 (1993).
25. E. J. Opila, D. L. Myers, N. S. Jacobson, I. M. B. Nielsen, D. F. Johnson, J. K. Olminky, and M. D. Allendorf, *J. Phys. Chem. A*, **111**, 1971 (2007).
26. J. Regina, J. DuPont, and A. Marder, *Mat. Sci. Eng. A*, **404**, 71 (2005).